POLITECNICO DI TORINO

Corso di Laurea in Ingegneria Aerospaziale

Prova finale

Lagrangian viewpoint of turbulent mixing in homogeneous isotropic turbulence and wall-bounded flows

Relatore:

Prof.ssa Stefania Scarsoglio

Candidato:

Steven Pisciotta Horner

Marzo 2021

Contents

Chapter 1

Introduction

Turbulence significantly amplifies mixing phenomena. In the past, much research has been devoted to the investigation of turbulent mixing from a chosen, fixed location. However, due to the crucial role of molecular transport in turbulent mixing, analyzing this phenomenon from the point of view of particles advected by the flow will grant a better insight into the processes occurring at the molecular level, which is where turbulent mixing ultimately occurs. This work is organized as follows: section 2 contains fundamental aspects regarding turbulence and the flows where investigations were performed; in section 3, turbulent mixing and its analysis in the Lagrangian framework are introduced; section 4 presents results originating from direct numerical simulations for turbulent dispersion, and most importantly for backward in time turbulent dispersion, where the trajectories of particles that arrive simultaneously at the same location are tracked for earlier times. Turbulent dispersion is investigated for pairs of passive tracers in homogeneous isotropic turbulence. Pairs of Brownian and inertial particles are then studied, and the additional effects due to molecular diffusivity and inertia are presented. Results for clusters containing three and four fluid particles are then illustrated, showing the evolution of parameters related to their sizes and shapes caused by turbulent dispersion. Finally, turbulent dispersion of pairs of particles is considered in wall-bounded flows, investigating the impact of the presence of boundaries on turbulent dispersion.

Chapter 2

Turbulence

2.1 Turbulent flows

The majority of fluid flows in nature and in engineering applications are turbulent [1]. Smoke emerging from a chimney, most atmospheric and oceanic currents, blood flowing through the arteries, are all examples of turbulence. Visually, turbulence appears as a superimposition of eddies whose sizes vary over a remarkably wide range of dimensions. Turbulence is a seemingly chaotic, three-dimensional, multiscale phenomenon, which features sudden and unpredictable variations in velocity and pressure. Therefore, all the properties of interest in turbulent flows are necessarily studied statistically. Another essential characteristic of turbulent flows is their extraordinary effectiveness in mixing mass, momentum and heat, rapidly dispersing these quantities throughout the fluid [1]. Despite the continuing research effort in turbulence, many aspects are still questioned, and a general solution to the turbulence problem has yet to be found.

2.2 Reynolds number and governing equations

The Reynolds number is defined as:

$$Re = \frac{UL}{\nu} \tag{2.1}$$

where U is the velocity, L is the characteristic length of the flow and ν is the kinematic viscosity of the fluid. It is a fundamental parameter in fluid dynamics, given by the ratio of inertial to viscous forces. When the Reynolds number is low, the flow is usually laminar: streamlines proceed parallel to one another with very little mixing between different layers. In this scenario, viscosity is effective in dampening perturbations, and the flow is able to remain laminar. As the Reynolds number increases in magnitude, the flow becomes turbulent, as the viscosity stops being able to dampen fluctuations. It is evident that laminar flows can only occur for moderate velocities, relatively small dimensions, or when the fluid's viscosity is large. Despite the well known unpredictability of turbulent flows, they are governed by a deterministic set of equations, the Navier-Stokes equations, which for an incompressible, Newtonian fluid are:

$$\frac{\partial \mathbf{u}}{\partial t} + \mathbf{u} \cdot \nabla \mathbf{u} = -\frac{1}{\rho}\nabla p + \nu \nabla^2 \mathbf{u} \tag{2.2}$$

$$\nabla \cdot \mathbf{u} = 0 \tag{2.3}$$

The reason behind the apparent randomness of turbulence is the strong nonlinearity in the Navier-Stokes equations, which makes turbulent flows extremely sensitive to perturbations: very small variations of the initial conditions can lead to significantly different characteristics in the flow.

The nonlinear term is also responsible for the the so-called energy cascade: kinetic energy is acquired by eddies at the largest scales of the flow, which are unstable and break up into smaller eddies several times, "passing down" the kinetic energy, until at the smallest scales of the flow viscosity is able to dissipate it into heat. Thus, another key characteristic of turbulent flows is that they are dissipative. Kolmogorov quantified these small scales [1]:

- $\eta = \left(\frac{\nu^3}{\varepsilon}\right)^{0.25}$ is the Kolmogorov lengthscale;

- $t_\eta = (\varepsilon\nu)^{0.5}$ is the Kolmogorov timescale;
- $u_\eta = (\varepsilon\nu)^{0.5}$ is the Kolmogorov velocity scale;

where ε is the dissipation rate of kinetic energy. Kolmogorov also showed that the ratio of these scales is dependent on the Reynolds number of the flow. If we define the large scales of the flow as l_0, t_0, u_0, then [1]:

- $\frac{\eta}{l_0} \sim Re^{-0.75}$
- $\frac{u_\eta}{u_0} \sim Re^{-0.25}$
- $\frac{t_\eta}{t_0} \sim Re^{-0.5}$

Increasing the Reynolds number increases the scale separation. Since the observation of asymptotic behaviors in turbulence requires adequate scale separation, experimental and numerical studies continuously try to increase the largest attainable Re.

2.3 Eulerian and Lagrangian frameworks

There are two possible viewpoints which can be adopted when studying a fluid flow. The most widespread is the Eulerian viewpoint: in this framework, a fixed in space set of coordinates is chosen, and the properties of the fluid are then sampled at different positions. Hence, properties of the flow depend on the location where they were sampled and on time. The alternative is the Lagrangian approach [2] [3], also referred to as the material viewpoint. In this case, the focus is placed on an infinitesimal volume of fluid which is identified through its position $\mathbf{x}_0$ at a certain time t_0 and tracked along its trajectory. Once the fluid particle is tagged with its initial location, properties only depend on time, and its current location becomes the origin of the coordinate system. In the Lagrangian framework, the variation of a certain property along a pathline is given by the material derivative $\frac{D}{Dt}$ [4]. This is equal to the time derivative computed in a certain point of the Eulerian framework with the addition of a convective term:

$$\frac{D}{Dt} = \frac{\partial}{\partial t} + \mathbf{u} \cdot \nabla \tag{2.4}$$

The presence of a convective term may significantly complicate certain problems, for instance the computation of fluid particle acceleration [2]. The Eulerian framework is generally preferred, since Eulerian data is typically easier to obtain than Lagrangian data, but determining the best approach depends on the problem at hand. In the case of turbulent dispersion, the Lagrangian viewpoint is a better option, since it inherently involves the tracking of particles transported by the flow.

2.4 Homogeneous Isotropic Turbulence

A turbulent flow is statistically homogeneous when its statistics are not affected by variations in space of the coordinate system. If it is invariant when the coordinate system is rotated or reflected as well, it is also isotropic [1]. Homogeneous isotropic turbulence (HIT) is the most simple and "pure" state of turbulence. HIT is not observed in nature or in industry. In wind tunnels, the flow which most accurately resembles HIT is grid turbulence. The flow is forced through a grid and quasi-isotropic, decaying turbulence is obtained in the core of the wind tunnel. Although HIT requires the absence of boundaries, sufficiently far away from the wind tunnel's walls the flow will be, with good approximation isotropic. In direct numerical simulations, due to computational power limitations, to obtain HIT the flow evolves in time instead of in space, relying on Taylor's frozen turbulence hypothesis.[5]

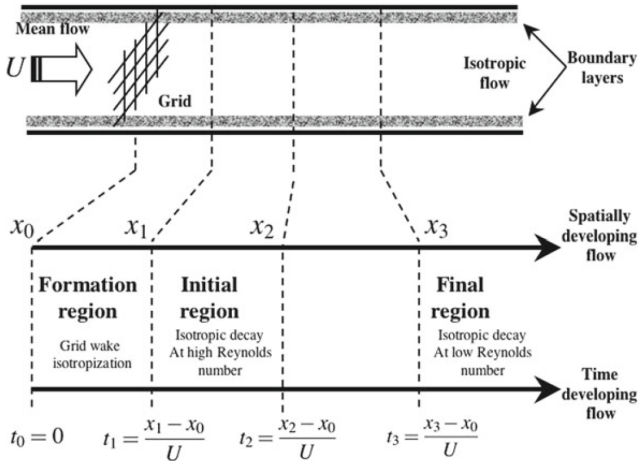

Figure 2.1 – Various regions in grid generated turbulence. From ref. [5]

2.5 Channel flow

Most turbulent flows present some type of boundary, thus homogeneity is generally lost. Much effort has been put into researching a few canonical wall bounded flows, namely channel flow, pipe flow and flat-plate boundary layer flow. In the first, the boundary is a rectangular duct, whose height 2δ is much smaller than the other two dimensions L (streamwise) and b (spanwise). Sufficiently downstream, the turbulent flow is fully developed and statistics no longer vary in the x direction. If the region considered is adequately distant from the vertical walls, statistics are independent of shifts in the z direction as well. Therefore, a statistically 1D flow is recovered, whose statistics depend exclusively on the y direction.

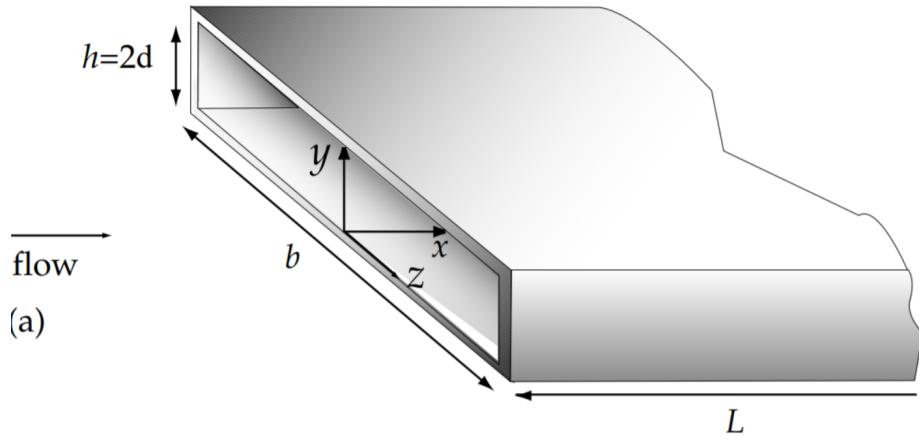

Figure 2.2 – Channel flow. From ref. [1]

The shear stress in the channel is given by:

$$\tau(y) = \rho\nu\frac{d\langle U\rangle}{dy} - \rho\langle uv\rangle \tag{2.5}$$

where $\rho\nu\frac{d\langle U\rangle}{dy}$ accounts for the shear stress due to viscosity and $-\rho\langle uv\rangle$, which is known as the Reynolds stress, accounts for the shear stress due to turbulent fluctuations. At the wall ($y = 0, y = 2\delta$), $\tau = \tau_w$, thus the shear stress is entirely due to the viscous contribution. As we move away from the boundaries, the Reynolds stress term becomes the main contribution. At the center of the channel, the shear stress vanishes, as shown in fig[2.3]

The following variables are then introduced: $u_\tau = \sqrt{\frac{\tau_w}{\rho}}$, $\delta_\nu = \frac{\nu}{u_\tau}$, respectively referred to

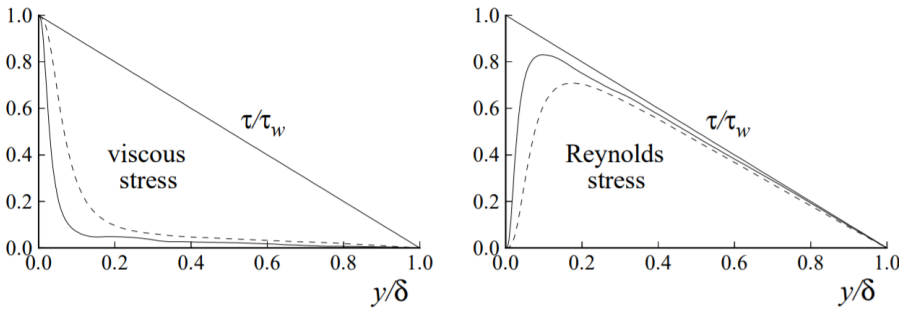

Figure 2.3 – Shear stress contributions as a function of the distance from the wall. From ref. [1]

as the friction velocity and viscous lengthscale. These can be used to obtain the following adimensional variables: $y^+ = \frac{y}{\delta_\nu}$, $U^+ = \frac{\langle U \rangle}{u_\tau}$, where $\langle U \rangle$ is the mean velocity in the channel. The laws which determine the value of U^+ depend on the distance from the wall in terms of y^+. For small values of y^+ , $U^+ = y^+$. This is valid up to $y^+ = 30$, after which the so called log-law holds:

$$U^+ = \frac{1}{k} \ln y^+ + B \tag{2.6}$$

In this equation, $k = 0.42$ is the Von Karman constant, and the value constant B is 5.2. The log-law maintains its validity up to $y \approx 1000$. Various zones can be identified in the channel [1]:

- Inner layer, for $\frac{y}{\delta} < 1$ the mean velocity depends exclusively on U_τ and y^+.
- Viscous sublayer, for $y^+ < 5$: the total shear stress is mostly due to viscosity.
- Buffer layer, for $5 < y^+ < 30$: layer in between the viscous sublayer and the log-law region. The contributions of viscosity and turbulent fluctuations are both significant in τ.
- log-law region: for $y > 30$, U^+ grows following the log law.

Chapter 3

Turbulent mixing and Lagrangian approach

3.1 Turbulent mixing

The ability to significantly enhance mixing phenomena is a fundamental feature of turbulent flows. Turbulent mixing occurs when a substance is introduced in a turbulent region, where the eddying motion exerts a stirring action across the whole spectrum of lengthscales of the flow. The interface area between the substance and the sorrounding fluid is increased and distorted, and local gradients are maintained, allowing mixing to progress much more rapidly than in a comparable laminar flow. Three categories of turbulent mixing may be identified [6]; the first encompasses instances where alterations of the fluid occur. This includes the majority of combustion phenomena, detonations, and supernovae. Changes in composition, enthalpy, pressure and density take place, often as a result of chemical reactions. These changes, in turn, alter (and significantly complicate) the dynamics of the flow, introducing further lengthscales and timescales. A second category of turbulent mixing may be identified when fluids with different density are mixed, but no alteration of the fluid occurs; also in this case, mixing alters the dynamics of the flow, as it decreases the density gradients within the flow. The simplest and most studied type of turbulent mixing is passive scalar mixing, i.e. the mixing of scalars which do not alter the flow dynamics. Two simple examples of passive scalar mixing are the mixing of

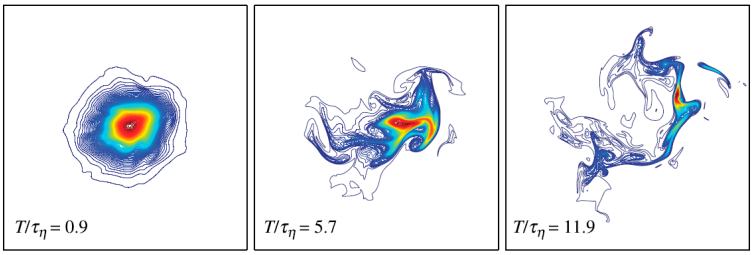

Figure 3.1 – Mixing of dye in a turbulent flow. From ref. [8]

dye in water and the mixing of fluids with small temperature differences (although if the temperature difference is significant, density is affected and the scalar can no longer be considered passive). Understanding the mixing of passive scalars is the first step in understanding more difficult instances of turbulent mixing. A qualitative example [7] is the mixing of a blob of dye in turbulent flow (fig.[3.1]). Initially it is a uniform bubble, and its probability density function corresponds to two delta functions at 0 and 1, respectively indicating the sorrounding uncontaminated fluid and the scalar. The scalar is then mixed with the sorrounding fluid by the turbulent eddying motions, and the two delta functions disappear, giving way to a central peak which indicates that the fluid and the scalar have mixed. Mixing of passive scalars is governed by the advection-diffusion equation:

$$\frac{\partial \theta}{\partial t} + \mathbf{u} \cdot \nabla \theta = K \nabla^2 \theta \tag{3.1}$$

where θ is the concentration of the scalar. This equation is linear in θ, but it is enormously complicated by the advective term, where the fluid velocity appears. Since the flow is turbulent, the advection-diffusion equation becomes a stochastic differential equation.

Effects of the Reynolds number

A transition Reynolds number is often encountered in turbulent mixing. For $Re \approx 10000$, the mixing is considered fully developed: mixing intensifies as the range of scales of eddying motion broadens and mixing becomes weakly dependent on Re [6].

Effects of the Schmidt number

The Schmidt number is defined as

$$Sc = \frac{\nu}{K} \tag{3.2}$$

where ν is the kinematic viscosity of the fluid and K is the molecular diffusivity of the scalar. The role of diffusivity is crucial in turbulent mixing. For mixing to occur, diffusivity must retain a finite value, because for $Sc \to \infty$ mixing at the small scales can not occur, as diffusivity ceases to even out the scalar concentration fluctuations. Therefore, the ability of turbulence to mix scalars weakens as Sc increases [9].

3.2 Lagrangian viewpoint of turbulent mixing

Most research in turbulent mixing has been carried out in the Eulerian framework. Adopting a Lagrangian framework [2] [3] has some downsides [7], since Lagrangian data is more difficult to acquired both experimentally and numerically. In the first case, Lagrangian data is typically obtained by optically tracking particles advected by the flow. This becomes increasingly challenging as the value of Re grows. Furthermore, these particles must be chosen with great care, ensuring that their trajectories accurately follow streamlines with negligible diffusive and inertial effects. In the second case, the difficulty arises from the massive computational requirements necessary to reach even moderate Reynolds numbers. Still, the Lagrangian framework has been shown to carry important benefits when investigating turbulent mixing. The basic underlying process of turbulent mixing is scalar transport by the turbulent flow [10]. In order to better understand and predict how substances will mix in a turbulent flow, the fundamental question to answer is how particles will separate and come together. This issue is naturally addressed in a Lagrangian framework, where the reference frame coincides with a particle advected by the flow. Choosing a Lagrangian framework also reduces the impact of random sweeping on scalar fluctuations. Random sweeping causes the smallest scales to be passively transported by the largest scales, when Re is large. This was shown to hold for passive scalars as well as for velocity [11]. Due to random sweeping, scalar fluctuations are much larger in the Eulerian framework than in the Lagrangian framework. Another advantage of adopting a Lagrangian viewpoint is that it allows to study a much wider range of values of Sc, avoiding the difficulties that emerge in the Eulerian framework when Sc is very small or very large [12]. Interest in Lagrangian investigations of turbulent mixing

has resurged in the last two decades, thanks to the improvements in experimental and computational methods to obtain Lagrangian data. Many theories in turbulence suggest the existence of asymptotic behaviors as the Reynolds number becomes infinitely large, and although reaching adequately high Reynolds number values is still a limiting factor, the currently attainable values make investigations of asymptotic behaviors worthwhile. The phenomenon addressed in the following chapter is turbulent dispersion, which is the fundamental process governing the spread of clouds of particles in fluids. If we consider two fluid particle whose locations are $\mathbf{x}_1$ and $\mathbf{x}_2$, their separation distance vector will be $\mathbf{r}(t) = \mathbf{x}_1(t) - \mathbf{x}_(t)$, with $\mathbf{r}_{t=0} = \mathbf{r}_0$ being the initial separation distance [13]. The relative velocity between the two fluid particles will be $\mathbf{w}(t) = \frac{d\mathbf{r}}{dt}$. To characterize how material will spread from a known source, the evolution of the distance of the pair of particles is of interest, however since the flow is turbulent we will of course be interested in a statistical quantity, the mean-square separation:

$$\langle r^2(t) \rangle = \langle \mathbf{r} \cdot \mathbf{r} \rangle \tag{3.3}$$

Where $\langle \cdot \rangle$ indicates an ensemble average over a large number of particles. The mean-square separation is one of the most investigated statistics in turbulent dispersion, because it effectively captures how clouds of particles spread in turbulence. It is a fundamental quantity of interest when studying relative dispersion, and several studies have been carried out to verify the existence of asymptotic laws governing its temporal evolution for different types of flows and different types of particles. However, turbulent mixing is quite the opposite of turbulent dispersion. In turbulent mixing, substances originating from different locations eventually coalesce and mix. From a molecular perspective, this is nothing but a time reversed dispersion process [14]: instead of considering a pair of particles which are initially located in close proximity of one another and separate as time goes by, we may consider a pair of particles originating from far locations which move closer to one another and at a later time T present a very small distance. Hence, if this pair of particles is considered at t = T and the trajectories of the two particles are tracked for earlier times, it essentially becomes a dispersion process. This is referred to as backward in time relative dispersion, and it is closely linked to turbulent mixing. Forward

and backward in time dispersion are similar processes for very short and very long times, while for intermediate times backward dispersion is generally faster. This asymmetry in time has been attributed to the direction of the flux of energy in turbulent flows, governed by the term $\mathbf{u} \cdot \nabla \mathbf{u}$ in the Navier-Stokes equations. Investigating backwards dispersion in turbulence is crucial to grasp the underlying physics which control turbulent mixing. It is also known that statistics from the trajectories of particles can be related to the statistical moments of the scalar field, and backward dispersion was shown to be closely linked to the dissipation of scalar fluctuations. In the particular case where the instantaneous scalar gradient source is uniform in direction z, $S(\mathbf{x}, t) = Gz\delta(t)$, the scalar dissipation χ could be written as a function of the time derivative of backward relative dispersion, adjusted for diffusion effects: $\chi = \frac{1}{2}G^2 \frac{d\langle r^2 \rangle}{dt} - 2G^2K$ [14].

3.3 Direct numerical simulations

Most Lagrangian data originates from direct numerical simulations (DNS) [15] [3]. In DNS, the Navier-Stokes equations are numerically solved over the entirety of spatial and temporal scales of the flow, without any modelling; hence, the computational power required is massive, as it grows $\sim Re^3$. To accurately resolve all scales, the grid must be larger than the largest lengthscale of the flow, $Nh > L$, but its spacing must be smaller than the smallest scales of the flow, $h < \eta$. Furthermore, the duration of the simulation must be longer than the integral timescale T_L of the flow, but the time step must be short enough that particles have advanced less that a grid step. In order to obtain the Lagrangian trajectories of particles, an Eulerian velocity field must first be available. Then, the Eulerian field is interpolated to obtain Lagrangian velocities of particles. Finally, by integrating Lagrangian velocities, particle trajectories are acquired.

Chapter 4

Results

4.1 Dispersion in HIT

The first case of interest is the dispersion of fluid particles [13] [16], also referred to as passive tracers, whose motion accurately follows the flow. Understanding the laws governing their motion in HIT is the first step in understanding more complex dispersion phenomena, such as when molecular diffusivity is present, or when inertial effects must be taken into account, or when the flow presents some type of boundary.

Three distinct regimes can be identified for $\langle r^2(t) \rangle$, namely the dissipation regime, for very small times and separation distances, the inertial regime, for intermediate times, and the diffusive regime, for long times. In the dissipation subrange particles separate exponentially, because their relative velocity increases as their relative distance increases. Hence, their separation evolves as [13]:

$$\langle r^2(t) \rangle \sim r_0^2 \exp(\xi t) \tag{4.1}$$

where $\xi = \frac{2B}{t_\eta}$, B is the Batchelor constant. In the dissipation subrange, the separation is dependant on the magnitude of the initial separation, therefore it is clear that two fluid particles whose initial distance is zero will never separate. If the particles present non-zero initial separation, for intermediate times they will exit the dissipative subrange and move to the inertial subrange. In the inertial subrange, the law governing the temporal

evolution of the mean-square separation distance is the following:

$$\langle |\mathbf{r}(t) - \mathbf{r}_0|^2 \rangle = \begin{cases} \frac{11}{3} C(\langle \varepsilon \rangle r_0)^{2/3} t^2 & \text{for } t << t_B \\ g \langle \varepsilon \rangle t^3 & \text{for } t_B << t << T_L \end{cases} \tag{4.2}$$

In this equation, $t_B = r_0^{2/3} \langle \varepsilon \rangle^{-1/3}$ is the Batchelor timescale, $\frac{11}{3} C(\langle \varepsilon \rangle r_0)^{2/3}$ is the second-order Eulerian structure function, g is known as the Richardson constant, which is believed to be universal, and C$\simeq$ 2.13 is also expected to be a universal constant. Two distinct behaviors for the mean-square separation exist in the inertial subrange: for very short times, $\langle |\mathbf{r}(t) - \mathbf{r}_0|^2 \rangle$ evolves in the Batchelor regime : the two particles maintain their initial velocity (which is the reason why it is also referred to as ballistic renge) as they move within an eddy of size $\sim r_0$, which requires $t \approx t_B$ to break up [17]. For longer times, the mean-square separation grows with $\sim t^3$ law in the Richardson-Obukhov super-diffusive regime. In the R-O regime, it is primarily eddies whose size $\approx r$ that are responsible for increasing the distance between the two tracers, and relative dispersion ceases to be influenced by the initial separation [13]. The $\sim t^3$ law stems from Richardson's so called 4/3 law for mixing and diffusion, and it is believed to be universal, since it regards the small scales of the flow [14]. This law considers the dispersion of particles as a diffusive process, whose diffusivity constant K is proportional to the distance between pairs of particles: $K \sim d^{4/3}$.

Finally, for long times the particles enter the diffusive subrange, where the mean-square separation increases linearly with time.

$$\langle |\mathbf{r}(t) - \mathbf{t}_0|^2 \rangle = 12 \sigma_u T_L t \qquad \text{for } t >> T_L \tag{4.3}$$

Where σ_u is the mean square component of the turbulent velocity. The regimes presented thus far refer to forward in time dispersion, but can be generalised to backward in time dispersion by substituting t with -t. It is backward dispersion, not forward, which is intimately linked with turbulent mixing.

4.1.1 Fluid Particles

The dispersion of passive tracers was investigated forward and backward in time [18]. The Taylor-Reynolds number $Re_\lambda = \frac{\langle \mathbf{u}'^2 \rangle \lambda}{\nu}$, where $\left(\langle \mathbf{u}'^2 \rangle\right)^{0.5}$ is the root mean square fluctuating velocity and $\lambda = \sqrt{15\frac{\nu\langle \mathbf{u}'^2 \rangle}{\varepsilon}}$ is the Taylor microscale, reached values up to 1000. The Reynolds number is pushed to the highest possible values to obtain a better separation of scales and therefore a clearer inertial subrange. The dissipation and diffusion subranges, on the other hand, are not dependent on how large the Reynolds number is in the simulation, but respectively depend on how small the time step used is and on the duration of the simulation. The particles were separated into various bins depending on the magnitude their initial separation r_0, regardless of their orientation, since in HIT only the magnitude of r_0 is relevant. Each bin included particles such that $2^{i-3} \leq \frac{r_0}{\eta} \leq 2^{i+1}$, with $i \in \mathbb{N}$, and was identified by $\frac{\tilde{r}_0}{\eta} = 2^{i-1}$.

Figure[4.1] shows the evolution of the mean square separation in time. For short times $t << t_B$ particles are in the ballistic subrange, and $\langle |\mathbf{r}^2 - \mathbf{r}_0^2| \rangle \sim t^2$. As expected, there was overlapping for forward and backward in time statistics. Once $t_B << t << T_L$, backwards relative dispersion proceeded at a faster pace than forward in time, which implies that the Richardson constant does not have the same value forward and backward in time. This asymmetry is attributed to the direction of the flux of energy in the flow.

For long times, forward and backward dispersion proceed similarly, with all curves converging to the linear growth law for $\langle |\mathbf{r}^2 - \mathbf{r}_0^2| \rangle$. This is clearer in simulations carried out for longer times. The value of the Richardson constant was sought, and the mean square separation, compensated for $\langle \varepsilon \rangle t^3$ was plotted as a function of time in figure[4.2]. The curves collapse onto a constant plateau for $t >> t_B$, increasingly so as Re_λ becomes larger. The initial separation is seen to influence how quickly the plateau is reached: for greater initial separations, the plateau was reached more rapidly, while for values of $\tilde{r}_0$ small enough to be in the dissipation subrange, viscous effects delayed the approach to the plateau. For backward relative dispersion, the effects of $\tilde{r}_0$ and Re_λ were the same as in forward dispersion, however since backward dispersion proceeds more rapidly in the inertial subrange, the plateau is reached sooner and has a larger value, as particle

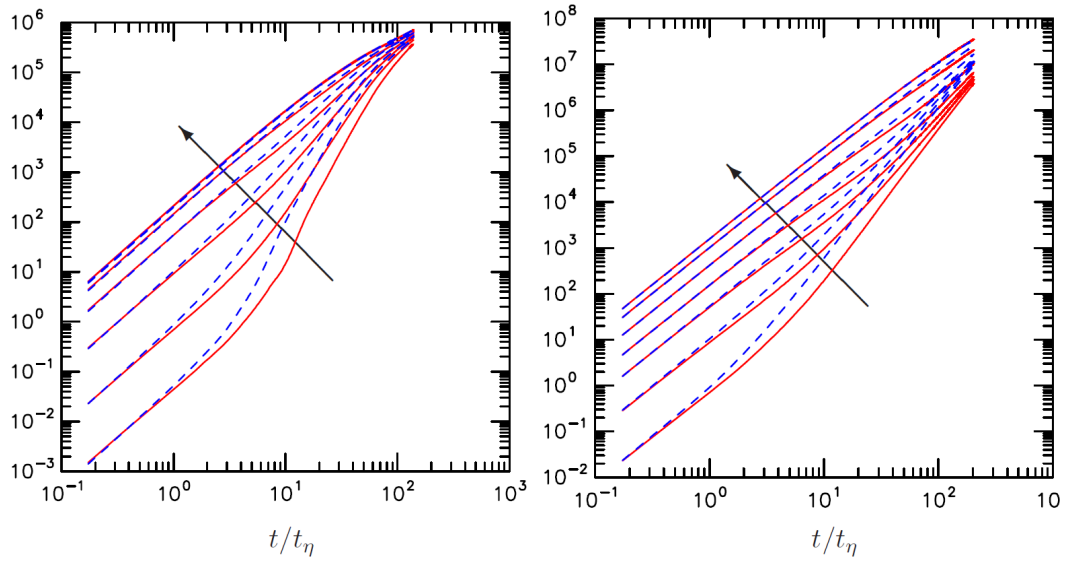

Figure 4.1 – The mean-squared relative displacement, scaled by the Kolmogorov lengthscale, is plotted as a function of time scaled by the Kolmogorov lengthscale, for $Re_\lambda = 140$ (left) and $Re_\lambda = 1000$ (right). The continuous red lines represent forward in time dispersion, while the dashed blue lines represent backwards in time dispersion. From ref. [16]

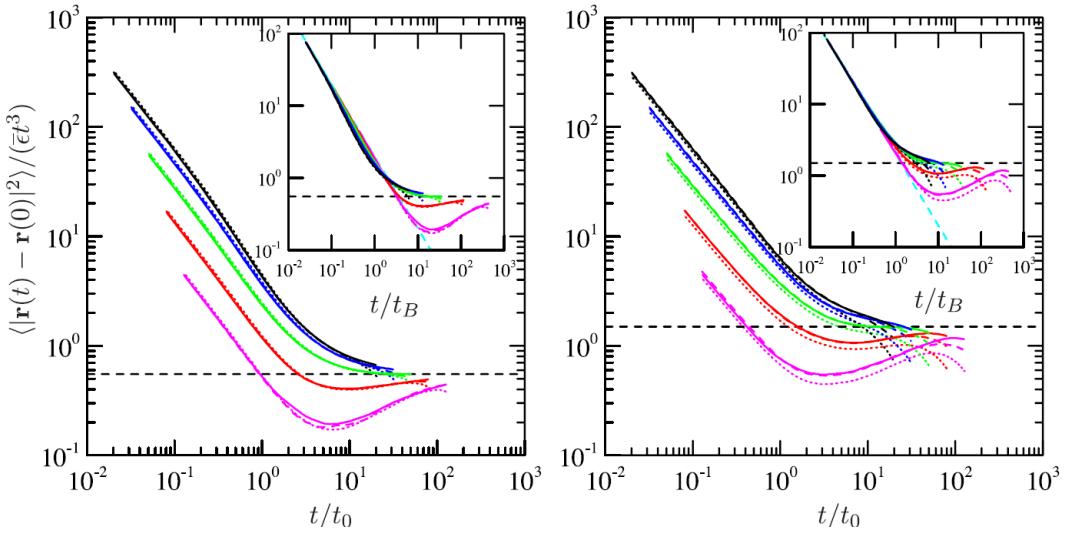

Figure 4.2 – Forward (left) and backward (right) in time compensated mean-square relative displacement as a function of time scaled by the Richardson timescale. The different colors indicate the bins to which the data belongs: $\frac{\tilde{r_0}}{\eta} = 1, 2, 8, 16$ (magenta, red, green, blue and black, respectively). Dotted, dashed and continuous lines indicate $Re_\lambda = 390, 650,$ and 1000, respectively. From ref. [16]

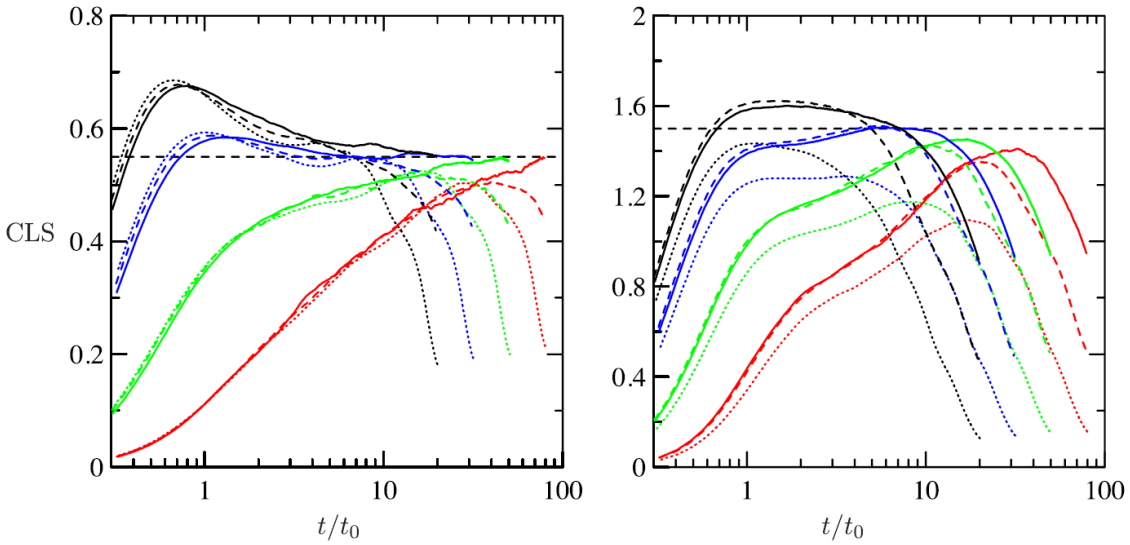

H

Figure 4.3 – CLS of mean-squared separation distance forward (left) and backward (right) in time. The conventions implemented to identify the value of the initial separation and Re_λ remain those presented in fig. [4.2]. From ref. [16]

pairs reach (and escape) the inertial range sooner. This plateau indicated the existence of Richardson scaling and also gave a hint of the value of the Richardson constant, however to obtain a more accurate value of g the cubed-local-slope (CLS) of the mean square separation, defined as $CLS = \frac{1}{\varepsilon}\left(\frac{d}{dt}[\langle r^2\rangle]^{1/3}\right)^3$ was plotted as a function of t/t_B (fig.[4.3]). Clearer plateaus were observed for this quantity, and the trends already observed for the compensated mean-square separation remained, showing the values for the Richardson constant forward and backward in time: $g_F = 0.55$ and $g_B = 1.5$.

4.1.2 Brownian particles

The relative dispersion of fluid particles in HIT has been a topic of great interest in research thanks to its relative simplicity, but usually, particles do not behave exactly as tracers. In general, particles transported by the turbulent flow also move under the influence of molecular diffusivity K. Excluding instances of very high molecular diffusivity, turbulent transport represents the stronger contribution to dispersion, if the Reynolds number is adequately large. In the limit Sc $\rightarrow \infty$, diffusivity effects are absent and we recover the behavior of fluid particles. The position of a particle whose motion is governed both by turbulent transport and molecular diffusion may be written by means of the following stochastic differential equation, which is the Lagrangian equivalent of the advection-diffusion equation:

$$d\mathbf{x}_m(t) = \mathbf{u}(\mathbf{x}_m(t), t)dt + \sqrt{2k}d\mathbf{W}(t) \tag{4.4}$$

where $\mathbf{x}_m(t)$ is the molecular position at time t, $\mathbf{u}(\mathbf{x}_m(t), t)$ is the instantaneous velocity evaluated at $\mathbf{x}_m(t)$, and $\mathbf{W}(t)$ is a standardized 3D Wiener process. The effect of molecular diffusivity on relative dispersion was studied with DNS [12]. Particles were separated in bins, similarly to the binning strategy used for fluid particles in the previous section. The Brownian motion was replicated in DNS by drawing Gaussian random numbers at every step. The mean-square relative separation was adjusted for molecular diffusion by subtracting 12Kt. Similarly to fluid particles, forward and backward dispersion were observed to overlap for very short and very long times, where convergence to diffusive regime was observed in all cases. A Taylor series expansion was obtained to characterize the mean-square separation at short times:

$$\frac{\langle|\mathbf{r}(t) - \mathbf{r}_0|^2\rangle}{\eta^2} = \left(\frac{r_0}{\eta}\right)^2 \left[\frac{1}{3}\left(\frac{t}{t_\eta}\right) - \frac{7}{18}\frac{S_\epsilon}{\sqrt{15}}\left(\frac{t}{t_\eta}\right)^3\right] + \frac{12}{Sc}\left[\frac{|t|}{t_\eta} + \frac{1}{9}\left(\frac{|t|}{t_\eta}\right)^3\right] \tag{4.5}$$

where the term S_ϵ is the dissipation skewness. This equation is valid so long as $t << t_\eta$ and $r << \eta$. The absolute value of time was considered in the second term on the right hand side of the equation, since this term does not change in backward in time dispersion. It was observed that both r_0 and Sc affected the dispersion of molecular pairs at early times. It is worthy of notice that, unlike fluid particles, when molecular

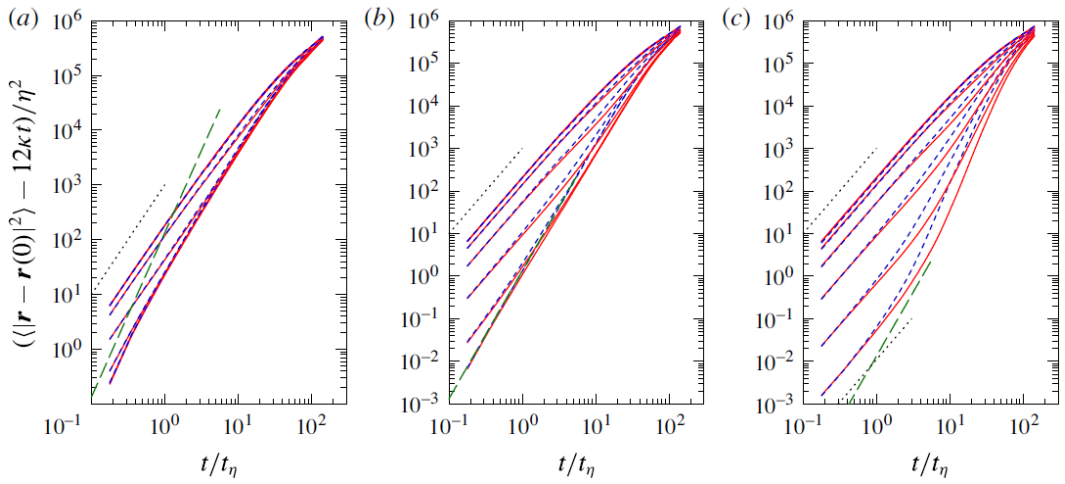

Figure 4.4 – Mean-square separation as a function of t/t_η at Re_λ for Sc = 0.01, 1, 100, respectively left, center and right. From ref. [12]

diffusivity is present, particles whose initial separation distance is zero will separate, as the first term in the right hand side of the equation will vanish, but the second will not. The effect of Sc is clear from the left panel: firstly, for low Sc and very small initial separation, the slope is steeper, indicating $\sim t^3$ growth for $\langle|\mathbf{r}(t) - \mathbf{r}_0|^2\rangle$, which was a consequence of the dominance of the second term of the right-hand side of equation(4.5) in these conditions. Secondly, reducing Sc reduces the difference between forward and backward in time dispersion. This was attributed to the fact that as Sc decreases, the Gaussian contribution to the particles' trajectories due to molecular diffusivity becomes larger. Since forward and backward dispersion would be the same for a Gaussian velocity field [14], when Sc decreases the difference between forward and backward dispersion diminishes. As Sc increases, the evolution in time of $\langle|\mathbf{r}(t) - \mathbf{r}_0|^2\rangle$ more closely resembles fluid particle behavior (center and right panel). At intermediate times, $\langle|\mathbf{r}(t) - \mathbf{r}_0|^2\rangle$ is expected to grow according to Richardson's law, therefore the CLS was studied, as already presented for fluid particles. In fig(4.5) the CLS is plotted for different values of Sc. For Sc $\to \infty$ and Sc = 1, the constant plateau maintained the value 0,55 already observed for fluid particles; for Sc = 0.125, the plateau was at 0,56. Backward in time, it was observed at 1,5 as in fluid particles, but a Sc dependence was observed: as Sc decreased, the value of the plateau decreased as well. The authors argued that larger values of Re would reduce this Sc dependence. Furthermore, as Sc decreased even further, Richardson

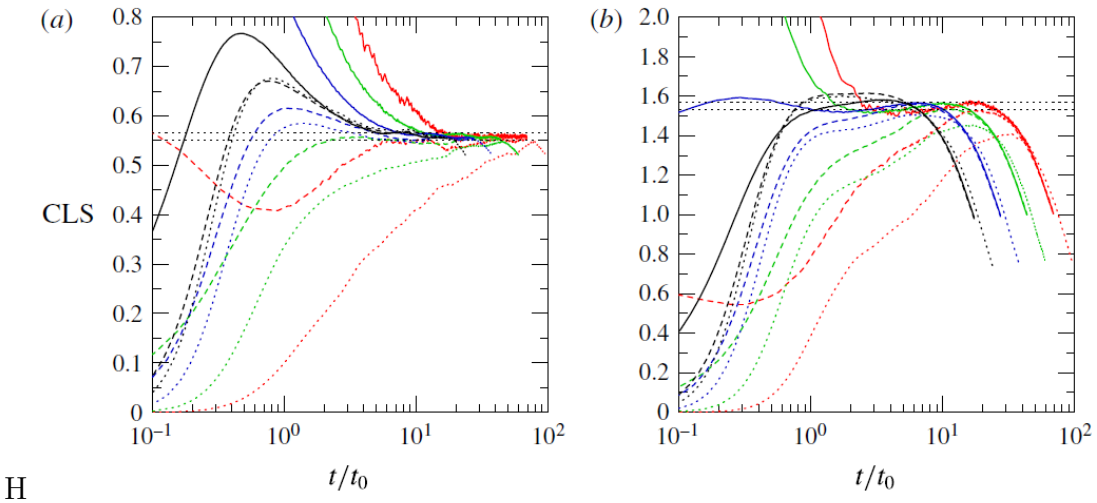

Figure 4.5 – CLS of the mean-square separation of Brownian particles. From ref. [12]

scaling was no longer observed, as the contribution of Brownian motion to the particle trajectories became too strong. Finally, for Sc ≈ 1, it was noticed that Richardson scaling was enhanced, since the diffusion contribution allowed particles to reach the Richardson regime sooner [16].

4.1.3 Inertial particles

A very common example of mixing of small particles whose density is much larger than the sorrounding fluid is given by water droplets in clouds, which leads to raindrop formation [19]. The dispersion of inertial particles differs from what was presented in section 4.1 for fluid particles because of additional complexities, such as preferential concentration, clustering and caustics. The inertial particles considered by the authors present densities much larger than the density of the sorrounding fluid, and their diameters are much smaller than the Kolmogorov length scale of the flow. To take into account how significantly the trajectories of inertial particles deviate from fluid particle pathlines, the Stokes number is introduced:

$$St = \frac{\rho_p D_p^2}{18\mu_g D_0/U_0} \tag{4.6}$$

where $\frac{\rho_p D_p^2}{18\mu_g} = t_p$ is the inertial particle's momentum response time [20], $\frac{D_0}{U_0}$ is a characteristic timescale of the flow, μ is the fluid's dynamic viscosity, ρ_p is the particle's density and D_p is its diameter. When St $\rightarrow$ 0, fluid particle behavior is recovered. When St ≈ 1, preferential concentration effects begin to manifest: heavy inertial particles escape regions of the flow which present high rotation and concentrate in regions of high strain. This causes an uneven distribution of the particles, which in incompressible HIT turbulence is not observed for fluid particles. As the value of St increases, the inertial particles will be less and less affected by the underlying flow. Inertial particles also tend to coagulate, forming clusters. This affects dispersion, since some particle pairs (especially lighter particles) may not separate at all due to clustering. Another mechanism which affects dispersion statistics is the formation of caustics [19] [21]. As a consequence, particles which are very close to one another may present significantly different velocities, instead of the velocity difference approaching zero as is seen with fluid particles. The formation of a caustic is shown in fig.[4.6]. The relative dispersion of inertial particles was investigated numerically forward [22] and backward [23] in time. The dispersion of inertial particles was seen to present two regimes: an extended ballistic regime, which continued well into the inertial subrange, after which the expected $\sim t^3$ behavior was observed. The first simulation [22] investigated forward relative dispersion of inertial particles, which were divided into two

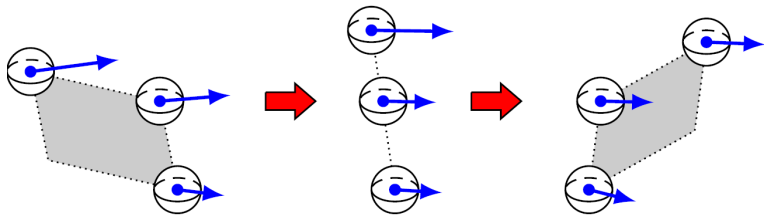

Figure 4.6 – 2D formation of a caustic: after initially forming a parallelogram, the particles align. From reference [21]

groups based on the value of their Stokes number: lighter particles presented St up to 3, while the Stokes number of heavy particles reached 70. In addition to the hypotheses on size and density of the particles, collisions were neglected and the particles were assumed not to alter the flow dynamics. The first run was performed at $Re_\lambda \approx 200$ and $St \leq 3,3$. The results were compared with analogous fluid particle dispersion (St = 0). It was observed that inertial particles initially separate more rapidly than fluid particles, and this was attributed to caustics: since the velocity differences between nearby inertial particles are much greater than the analogous velocity differences observed in nearby fluid particles, separation is enhanced for the former. The transient ballistic regime $\sim t^2$ was amplified as the value of St increased. This ballistic regime was affected by the initial separation of inertial particles, and in particular by how small the initial separation r_0 was compared to the lengthscale typical of caustics $R^* = \eta St^{3/2}$. For larger initial separations, the deviation from fluid particle behavior observed at early times significantly decreased, as the local velocity differences between inertial particles with respect to the sorrounding fluid were mitigated. For longer times, once the separation of inertial particles had become larger than R^*, their separation proceeded $\sim t^3$, similarly to fluid particles. Eventually, fluid particle dispersion overtook inertial particle dispersion. Although this is not clearly visible in fig[4.8] due to the limitations on the duration of the simulation, it was explained by the fact that the particles' inertia caused them to be affected by the fluid velocities they experienced at prior locations; however, the fluid velocity difference at previous locations was usually smaller than the fluid velocity difference at the locations where the inertial particles currently were. In the second run, Re_λ was increased and so were the

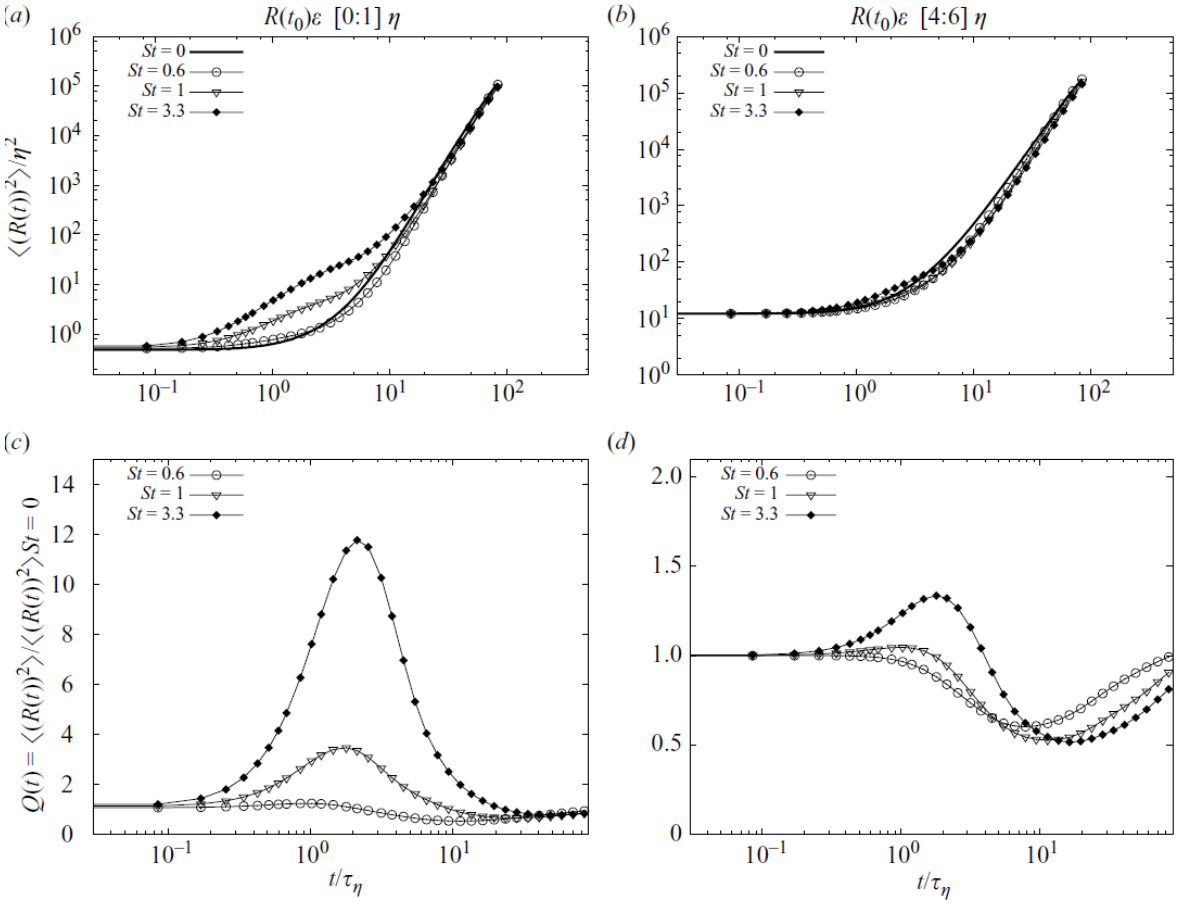

Figure 4.7 – Mean-square separation for inertial particles as a function of t/t_η, for various initial separations: $r_0 \approx \eta(a) 4\eta \leq r_0 \leq 6\eta(b)$. In (c) and (d) the mean-square separation of inertial particles is compared to fluid particle mean-square dispersion. First run, from ref. [22]

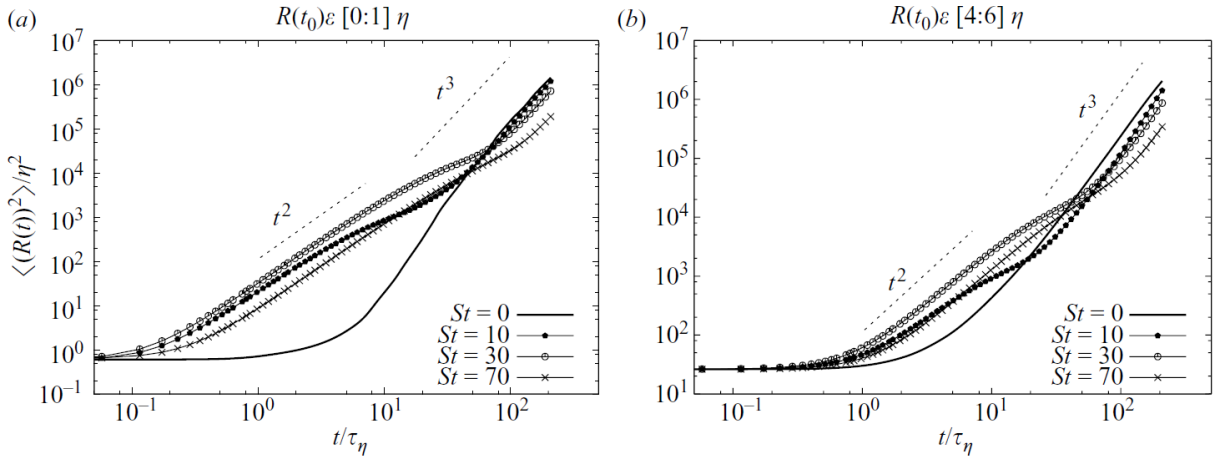

Figure 4.8 – Mean-square separation statistics from second run; the initial distances remained unchanged, while St went up to 70 and Re_λ increased to 400. From ref. [22]

values of St. An even stronger deviation from fluid particle dispersion was observed, and for the largest values of St the inertial particles never recovered $\sim t^3$ dispersion, even for larger initial separations.

A second investigation [23] studied the backwards dispersion of inertial particles. The results they obtained for forward dispersion were very similar to those from ref. [22]. Faster backwards dispersion was observed for inertial particles than for tracers. Due to inertia, when particles approached each other at small scales, memory of the velocities of the sorrounding fluid they encountered at larger scales, from which the particles were originating, was retained. This effect increased as St grew, due to the increasing relevance of inertial effects. This "memory" due to inertia, which caused fluid particle dispersion to eventually overtake inertial particle dispersion forward in time, caused inertial particles to approach each other more rapidly than fluid particles at intermediate and short times. The authors explained that the duration of the simulation was not long enough to observe long time behavior, although inertial particles are expected to approach each other more slowly than fluid particles at large times. The temporal asymmetry is stronger for inertial particles: due to non-local dynamics, i.e. due to the influence that earlier fluid velocities exert on inertial particle's present velocities, a new irreversibility mechanism arises [23]. This mechanism is in addition to the temporal irreversibility mechanism originating from the direction of the energy cascade. The ratio of backward mean square separation of

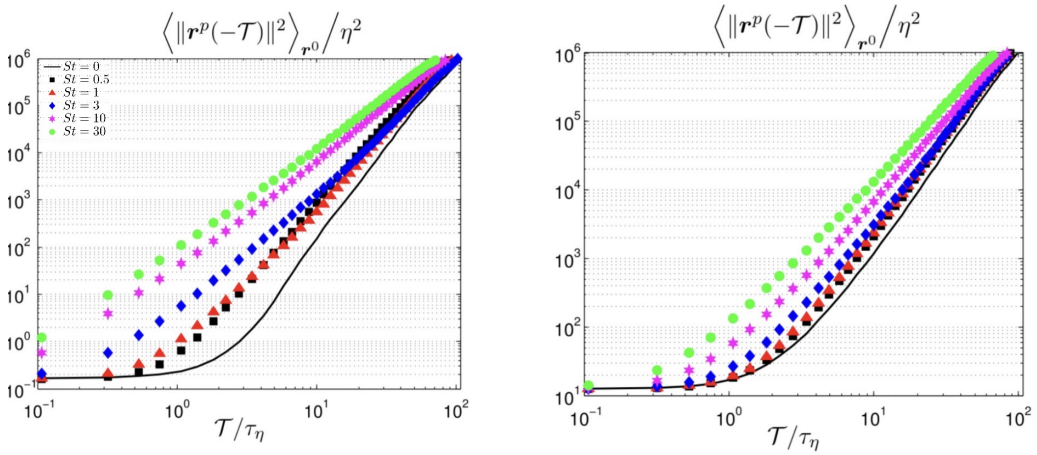

Figure 4.9 – Backward dispersion of inertial particle pairs for various St. The initial separation r_0 is $\in [0, 25\eta; 0, 5\eta]$ in the left panel and $\in [3\eta, 4\eta]$ in the right panel. From ref. [23]

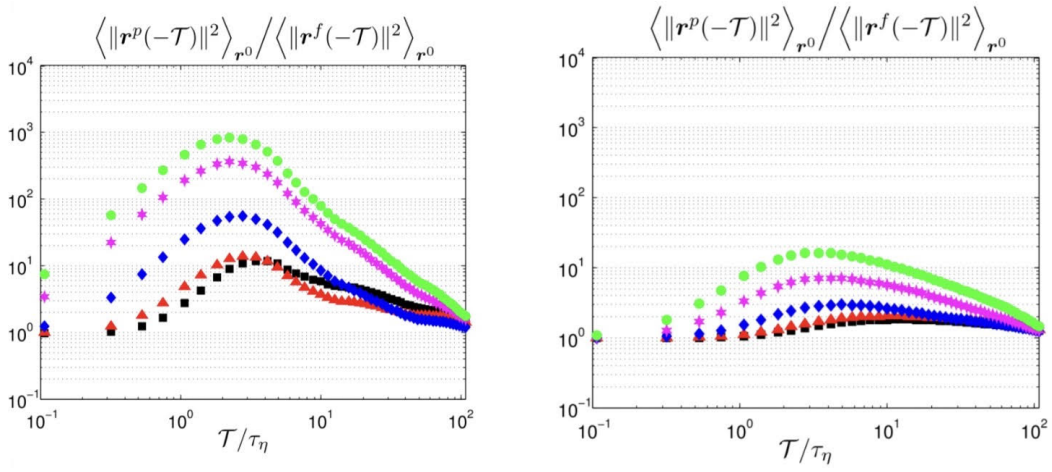

Figure 4.10 – Ratio of inertial to fluid particle backward mean square separation. The grouping of particles is the same as in fig.[4.9] From ref. [23]

inertial and fluid particles is shown in figure(4.10).

4.1.4 Multi-particle dispersion

Studies regarding the dispersion statistics of larger groups of particles have been carried out in HIT. These particle clusters are referred to as triangles and tetrads, respectively groups of three and four fluid particles. The dispersion statistics of triangles and tetrads grant insight into how turbulent dispersion affects shapes and volumes. Furthermore, since the n-th moment of the scalar field is linked to the dispersion statistics of groups of n particles, triangle and tetrad dispersion allow to obtain the third and fourth moments of the scalar field. Similarly to the investigations presented in previous sections, the existence of inertial scaling behaviors was sought. To characterize the particle group, the separation vectors are defined:

$$\rho_1 = \frac{1}{\sqrt{2}}(\mathbf{x}_2 - \mathbf{x})$$

$$\rho_2 = \frac{1}{\sqrt{6}}(2\mathbf{x}_3 - \mathbf{x}_2 - \mathbf{x}_1)$$

$$\rho_3 = \frac{1}{\sqrt{12}}(3\mathbf{x}_4 - \mathbf{x}_3 - \mathbf{x}_2 - \mathbf{x}_1)$$

where $\mathbf{x}_m$ is the position of the m-th particle. Two are necessary for triangles, three are necessary for tetrads. The matrix ρ is then defined: its i-th column is given by ρ_i. This matrix will be used to define the moment of inertia tensor M, given by multiplying ρ by its transpose. The diagonal elements of M, g_i, are its eigenvalues. Subsequently, the following quantities are introduced [24]:

- $R^2 = \sum g_i = \sum_{m=1}^{n-1} |\rho^m|$ represents the size of the cluster;
- $w = \frac{4A}{\sqrt{3}R^2}$, where A is the surface of the triangle formed by three particles, is a parameter that represents the aspect ratio of triangles;
- $V = \frac{1}{3}\sqrt{g_1 g_2 g_3}$ is the volume of tetrads;
- $\Lambda = \frac{V^{2/3}}{r^3}$ is a parameter which accounts for the shape deformation: its maximum value is 0.16025, which corresponds to a regular tetrahedron, while deformations of the shape cause its value to decrease.

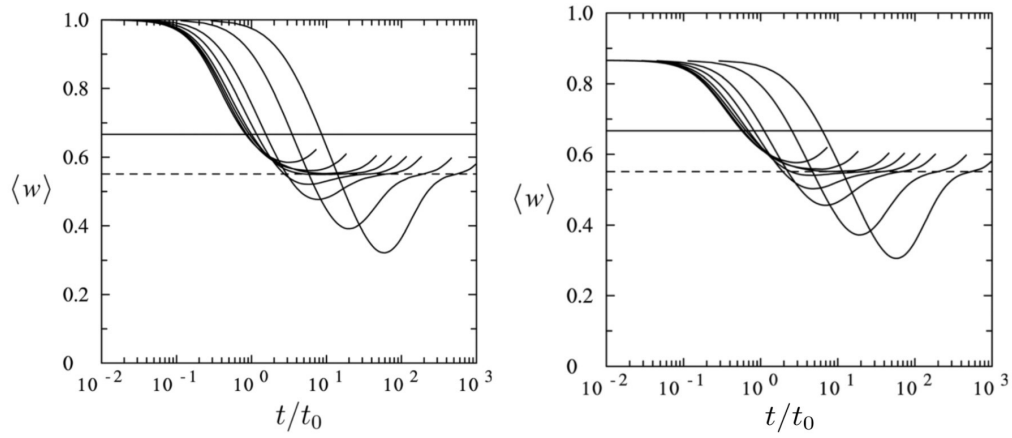

Figure 4.11 – Inertial subrange scaling at $Re_\lambda = 1000$ for triangles for different values of r_0 larger r_0 terminate at earlier times. From ref.[25]

Inertial subrange scaling was investigated for all of these quantities in various studies [25] [18] The area of triangles and the volume of tetrads, averaged over large ensembles of particles, are expected to scale as[10]:

- $\langle V \rangle \approx \langle \varepsilon \rangle^{3/2} t^{9/2}$
- $\langle A \rangle \approx \langle \varepsilon \rangle t^3$

Most studies regarding clusters of fluid particles investigated tetrads rather than triangles, since the statistics from tetrad dispersion grant better insight into shape distortion caused by turbulent dispersion [25]. Inertial subrange scaling was sought for the aspect ratio parameter of triangles. Two types of initial configurations were considered, namely rectangular isosceles triangles and equilateral triangles, at $Re_\lambda = 1000$. Numerous values of r_0, i.e. the length of the equal side in the case of isosceles triangles, or the length of all sides in the case of equilateral triangles. Some inertial range scaling was observed in all cases: inflection points in proximity of $\langle w \rangle$ were observed, indicating that for a certain time interval this parameter tended to maintain a constant value. The results for the statistics tetrad dispersion in HIT forward and backward in time are now presented [9]. The dispersion of tetrads grants statistics for size, as well as for shape, evolution caused by turbulent dispersion. Multiple previous studies [25] [24] have shown the presence of inertial range scaling for shape as well as size statistics of fluid particle tetrads, but that

it is clearer in the case of shape statistics.

The dataset employed was the same considered in ref. [16] for fluid particle pair dispersion. The results which emerged for temporal asymmetry of statistics relating to the sizes of clusters were qualitatively similar to those observed for fluid particle pairs: the temporal asymmetry manifested for intermediate times, with stronger backward in time dispersion. Governing equations for the mean square gyration radius $\langle R^2 \rangle$ were obtained by simply multiplying the laws for the ballistic, inertial and diffusive regime previously obtained for fluid particle pairs by $\frac{3}{2}$. This consideration arose from the definition of R^2 and from the fact that, initially, the tetrahedron is regular, so its 6 sides, and therefore the six distances between the various fluid particle pairs contained in the cluster were all equal. Since the focus remained on inertial range scaling, based on the previous assumption, the CLS of $\langle R^2 \rangle$ was expected to plateau for $\frac{3}{2}g$, thus a plateau $\approx 0,825$ forward in time and $\approx 2,25$ backward in time were predicted. The $CLS = \frac{1}{\varepsilon}\left(\frac{d}{dt}[\langle R^2 \rangle]^{1/3}\right)^3$ was plotted as a function of t/t_B. Forward in time, a plateau was clearly observable for 0,85, but backward in time the scaling was much weaker. A horizontal line was drawn for 2,25 for backward in time dispersion, showing that the CLS approached it only for very brief periods of time. The author argued that larger a larger Reynolds number was necessary to observe a clear plateau backward in time. As other researches pointed out, scaling is generally clearer for statistics regarding the shape of clusters. Thus, the mean of Λ is presented as a function of t/t_B; In the case of Λ, the temporal asymmetry appears to be reversed, as it is smaller backward in time. However, Λ does not represent a length: it is a parameter whose value $\in [0; 0,16025]$, which has its largest value for a regular tetrahedron and whose value decreases as the shape is distorted. Therefore, smaller Λ backward in time, indicates that the shape distortion is stronger in this case.

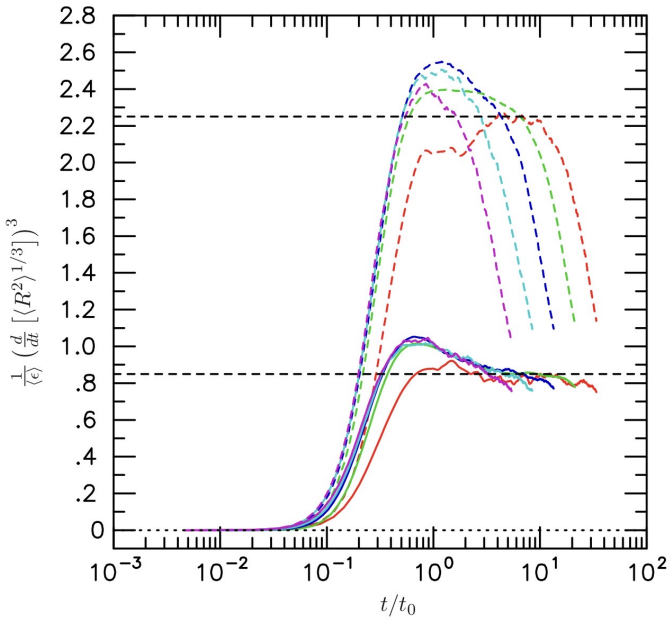

Figure 4.12 – CLS of $\langle R^2 \rangle$ forward and backward in time (respectively, continuous and dashed lines). From ref.[18]

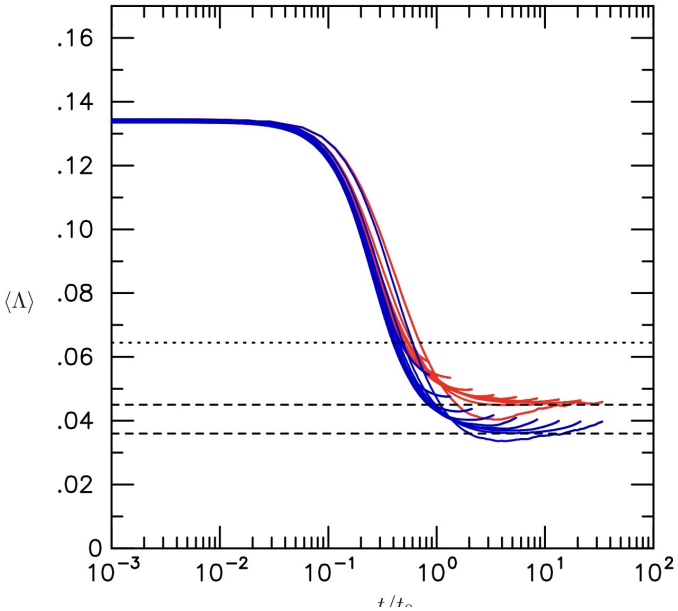

Figure 4.13 – Forward and backward (respectively, red and blue) in time Λ for various initial r_0 at Re_λ = 1000. Curves for larger r_0 terminate at earlier times. From ref. [18]

4.2 Channel flow

Although most research devoted to dispersion in turbulence has focused on isotropic turbulence, this is an ideal setting and the effects of boundaries on dispersion must be considered. However these boundaries carry additional complications. Firstly, the flow inhomogeneous, especially in proximity of the walls where mean shear is dominant (while a certain degree of homogeneity in the core of the channel is recovered). Secondly, in addition to the magnitude of the initial separation of a pair of particles, its orientation and the distance from the wall must be considered. Thirdly, the scales of the flow vary in the wall-normal direction, and therefore it is possible for two pairs of particles whose separation is the same to belong to different regimes [26]. In all cases it was observed that particle separation was much larger streamwise than in the other directions. Although this was in part due to mean shear, which boosted particle separation, the authors [26] argued that a significant contribution came from more intense turbulent fluctuations in the streamwise direction.

4.2.1 Fluid particles

The numerical data presented is from two numerical studies: in ref. [27], the dispersion of fluid particles was studied forward and backward in time, while ref. [26] investigated the dispersion of fluid and inertial particles forward in time at $Re_\tau \approx 150$. The dispersion of fluid particles was studied in DNS. In both cases, the domain was a rectangular box, periodic in the streamwise and spanwise directions, whose dimensions were: $L_x \times L_y \times L_z = 4\pi h \times 2\pi h \times 2h$. Two datasets were implemented [27]: the first one initialized tracers at random locations, but dispersion was also studied backward in time, while the second one initialized the fluid particles at selected locations to study the effects of initial separation. The friction Reynolds number was $Re_\tau \approx 1440$. The coordinate system implemented in the two cases differs, as in ref. [26] the wall-normal direction is z, while in ref. [27] the wall-normal direction is y. In figure[4.14] the mean-square separation was plotted as a function of the crossing time, i.e. the time required for a particle in the center of the channel to cover the entire streamwise distance. Three wall distances are shown in figure[4.14]. Very

near the wall(a), the pairs which separate more rapidly are the ones whose initial distance $\mathbf{d}_0$ is in the wall-normal direction. The impact of the orientation of $\mathbf{d}_0$ weakens as the distance from the wall grows (c,e). The largest separation was observed for initial distance from the wall $z^+ = 37$, where Reynolds stress was largest. Fig.[4.15] shows the effect of the orientation of the orientation of the initial distance of two particle pairs on their separation: the pair whose initial separation is in the wall-normal direction separates more rapidly. In ref. [27], the mean-square change of separation $\langle \mathbf{r}^2(t) \rangle = \langle (\mathbf{d}(t) - \mathbf{d}_0)^2 \rangle$ was considered forward and backward in time in the first dataset. Its evolution (fig.[4.16]) was qualitatively similar to the results already shown in HIT, with overlapping data for short times, faster backward dispersion at intermediate times, and hinting an overlap for longer times. Richardson scaling was not observed due to the lack of scale separation.

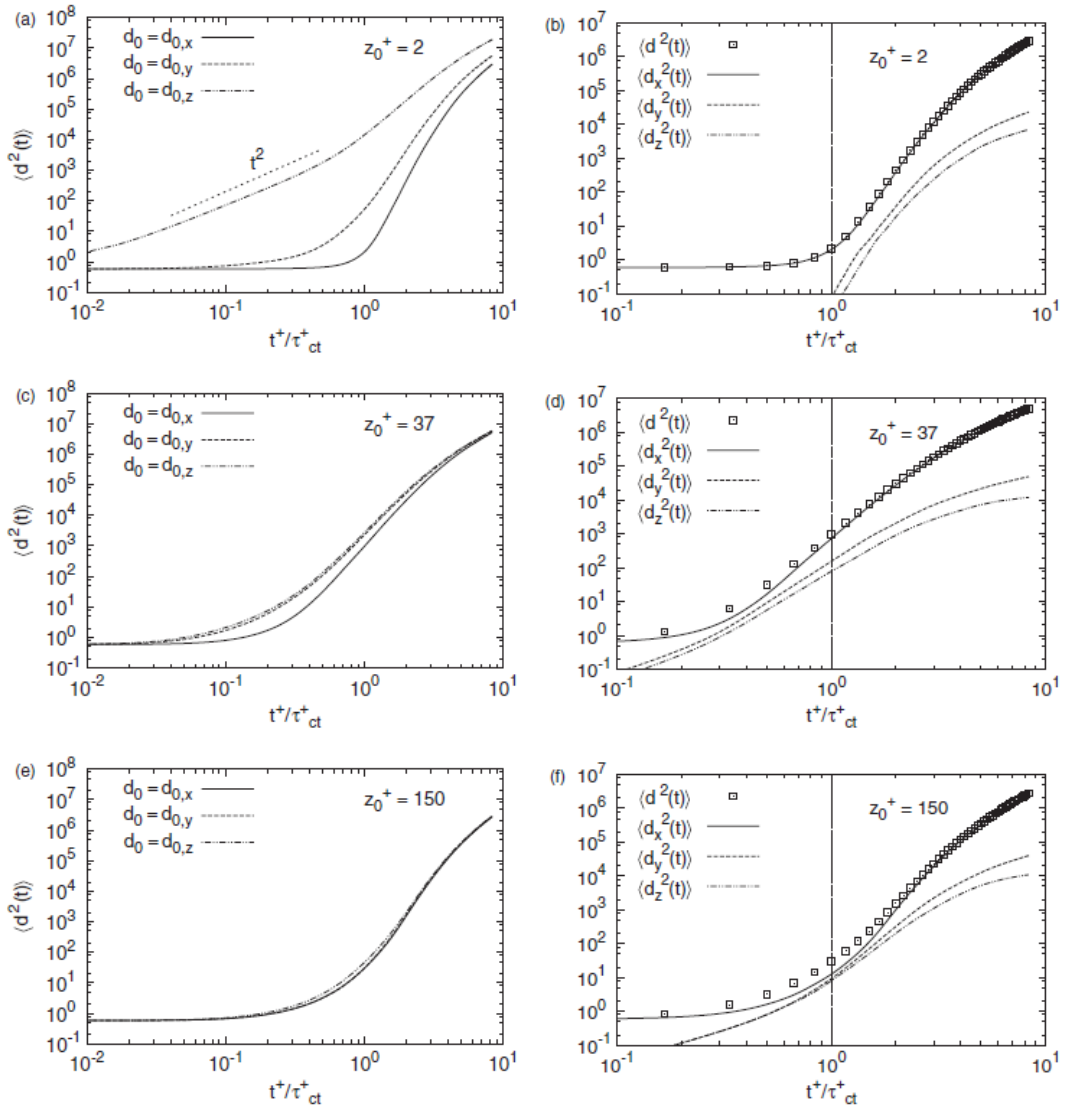

Figure 4.14 – Mean-square separation of fluid particle pairs for various wall distances. On the left, the effect of the orientation of the initial separation is shown; on the right, the growth of the components of the mean-square separation in the three directions is shown. From ref. [26]

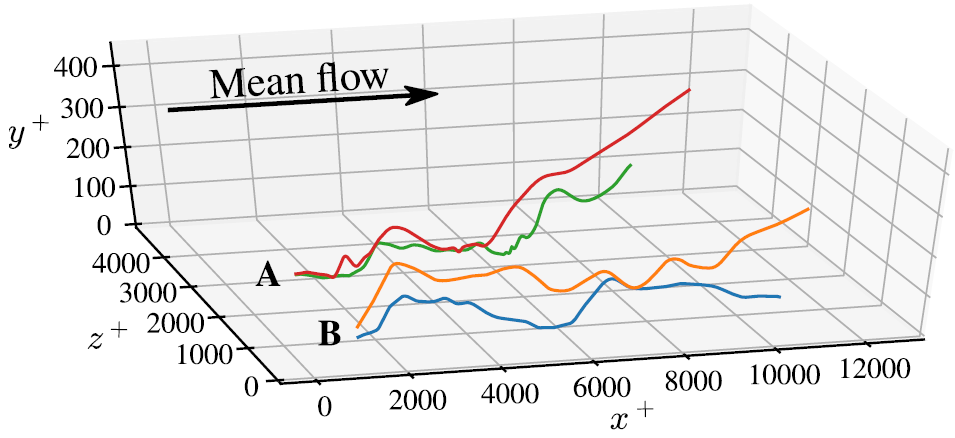

Figure 4.15 – Trajectories of two pairs of particles, whose initial distance differs only in orientation: pair A's initial separation is parallel to the wall, pair B's is wall-normal. From ref. [27]

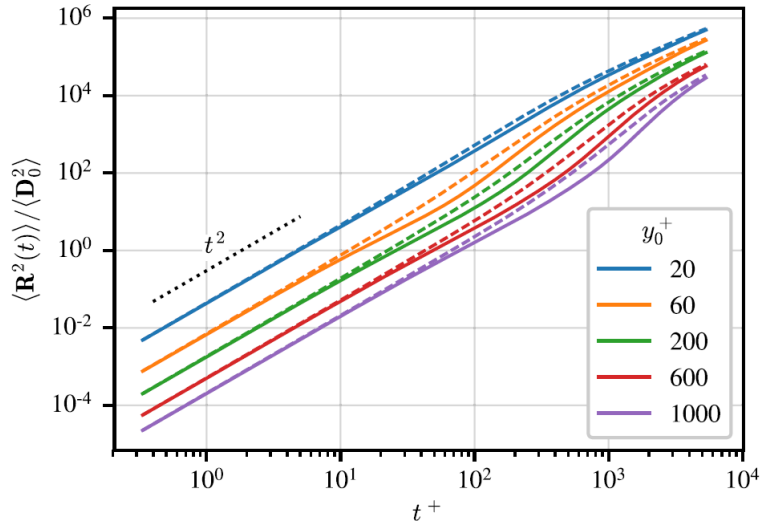

Figure 4.16 – Growth of $\langle \mathbf{r}^2(t) \rangle$ forward and backward in time for various initial distances from the wall. From ref. [27]

4.2.2 Inertial Particles

The statistics obtained for fluid particles in ref. [26] were used reference for the dispersion of inertial particles with St = 25. The particles were grouped based on their initial separation (considering its magnitude as well as its orientation) and on their Stokes number. Some similarities with fluid particle dispersion remained, namely the effect of initial wall-normal separation when pairs were placed near the wall, which still significantly boosted streamwise dispersion, and the maximum dispersion was also achieved when particles were placed in the region of maximum Reynolds stress. The following differences were observed: inertial particle pairs separated much more rapidly than fluid particles when initially placed near the wall. A slightly quicker separation of inertial particles was also observed when placed in the region of maximum Reynolds stress, although with a certain lag time. In the core of the channel this trend was reversed and fluid particle dispersion became faster. This different behavior, dependent on the initial distance from the wall, was explained by the tendency of inertial particles to escape regions of vorticity because of centrifugal force. When inertial particles entered streamwise oriented vortices near the wall, they were ejected in the wall-normal direction, therefore experiencing larger fluid velocity differences than tracers.

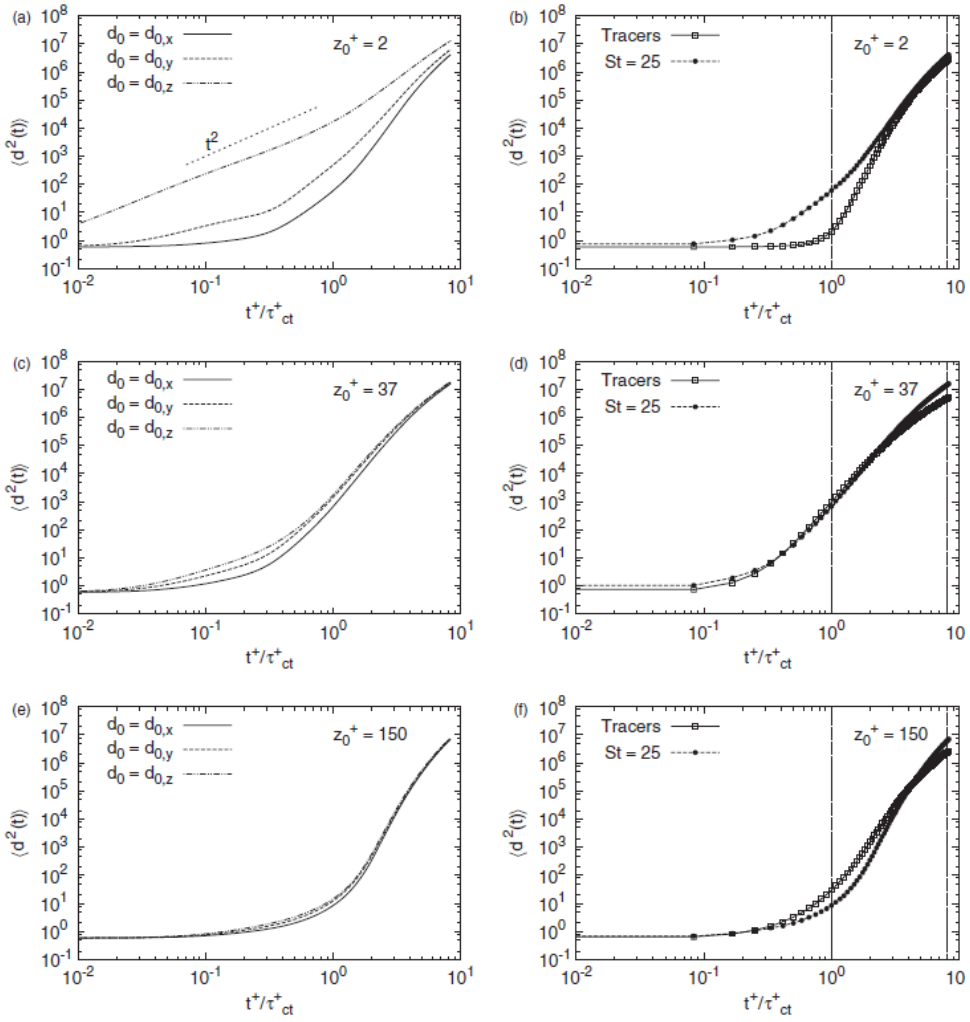

Figure 4.17 – Growth of the mean-square separation for St=25 and three different values of the initial wall distance. From ref. [26]

Conclusions

The Lagrangian viewpoint has proven to be better suited for the the investigations of turbulent mixing. Understanding the processes that govern the motion of particles will allow a more accurate description of the statistics of molecular trajectories, driving the development of more accurate models to predict the statistics of scalar fields. Much effort has been put into the investigation of passive scalar mixing, which is instrumental in understanding more complex categories of turbulent mixing. In this work, Lagrangian investigations of particle dispersion forward and backward in time have been presented. The latter has been shown to be intimately connected to turbulent mixing. It was observed that in general, forward and backward dispersion proceed similarly for short and long times, while an asymmetry in time is present for intermediate times. The underlying cause of this asymmetry was identified in the energy cascade, although inertial particles were shown to present an additional irreversibility mechanism. Evidence in favor of Richardson scaling was presented in the cases of pairs and clusters of fluid particles, as well as particles subjected to Brownian motion. Inertial particles exhibited an extended ballistic regime caused by caustics, eventually recovering $\sim t^3$ scaling if their Stokes number was not too large. In turbulent channel flows, particle separation was stronger in the streamwise direction, partly due to mean shear and partly due to stronger turbulent fluctuations in the streamwise direction. The temporal asymmetry in particle dispersion was present also in this case, but no Richardson scaling was observed due to the lack of scale separation. Further investigations may focus on the effects of low density and larger particle sizes on inertial particle turbulent dispersion; more accurate numerical investigations will be possible thanks to the steady increase over time of computational power. This will allow a better understanding of turbulent mixing at the molecular level, and consequently, the development of more accurate descriptions of mixing phenomena.

Bibliography

[1] Stephen B Pope. Turbulent flows, 2001.

[2] Federico Toschi and Eberhard Bodenschatz. Lagrangian properties of particles in turbulence. *Annual review of fluid mechanics*, 41:375–404, 2009.

[3] PK Yeung. Lagrangian investigations of turbulence. *Annual review of fluid mechanics*, 34(1):115–142, 2002.

[4] Juan Ignacio Polanco. *Lagrangian properties of turbulent channel flow: a numerical study*. PhD thesis, Université de Lyon, 2019.

[5] Pierre Sagaut and Claude Cambon. *Homogeneous turbulence dynamics*, volume 10. Springer, 2008.

[6] Paul E Dimotakis. Turbulent mixing. *Annual Review of Fluid Mechanics*, 37:329–356, 2005.

[7] Katepalli R Sreenivasan and Jörg Schumacher. Lagrangian views on turbulent mixing of passive scalars. *Philosophical Transactions of the Royal Society A: Mathematical, Physical and Engineering Sciences*, 368(1916):1561–1577, 2010.

[8] Katepalli R Sreenivasan. Turbulent mixing: A perspective. *Proceedings of the National Academy of Sciences*, 116(37):18175–18183, 2019.

[9] Dhawal Buaria, Matthew P Clay, Katepalli R Sreenivasan, and PK Yeung. Turbulence is an ineffective mixer when schmidt numbers are large. *arXiv preprint arXiv:2004.06202*, 2020.

[10] Peter A Davidson, Yukio Kaneda, and Katepalli R Sreenivasan. *Ten chapters in turbulence*. Cambridge University Press, 2012.

[11] PK Yeung and Brian L Sawford. Random-sweeping hypothesis for passive scalars in isotropic turbulence. *Journal of Fluid Mechanics*, 459:129, 2002.

[12] D Buaria, PK Yeung, and BL Sawford. A lagrangian study of turbulent mixing: forward and backward dispersion of molecular trajectories in isotropic turbulence. *Journal of Fluid Mechanics*, 799:352, 2016.

[13] Juan PLC Salazar and Lance R Collins. Two-particle dispersion in isotropic turbulent flows. *Annual review of fluid mechanics*, 41:405–432, 2009.

[14] Brian L Sawford, PK Yeung, and Michael S Borgas. Comparison of backwards and forwards relative dispersion in turbulence. *Physics of Fluids*, 17(9):095109, 2005.

[15] Wikipedia. direct numerical simulations, 2020.

[16] Dhawal Buaria, Brian L Sawford, and Pui-Kuen Yeung. Characteristics of backward and forward two-particle relative dispersion in turbulence at different reynolds numbers. *Physics of Fluids*, 27(10):105101, 2015.

[17] Abdallah Daddi Moussa Ider. Particle pair dispersion in 3d homogeneous isotropic turbulence. 2014.

[18] Dhawal Buaria. *Lagrangian investigations of turbulent dispersion and mixing using Petascale computing*. PhD thesis, Georgia Institute of Technology, 2016.

[19] M Wilkinson and Bernhard Mehlig. Caustics in turbulent aerosols. *EPL (Europhysics Letters)*, 71(2):186, 2005.

[20] Gabriel D Roy. Combustion processes in propulsion.

[21] Jan Meibohm, Vikash Pandey, Akshay Bhatnagar, Kristian Gustavsson, Dhrubaditya Mitra, Prasad Perlekar, and Bernhard Mehlig. Paths to caustic formation in turbulent aerosols. *arXiv preprint arXiv:2012.08424*, 2020.

[22] J Bec, L Biferale, AS Lanotte, Andrea Scagliarini, and F Toschi. Turbulent pair dispersion of inertial particles. *arXiv preprint arXiv:0904.2314*, 2009.

[23] Andrew D Bragg, Peter J Ireland, and Lance R Collins. Forward and backward in time dispersion of fluid and inertial particles in isotropic turbulence. *Physics of Fluids*, 28(1):013305, 2016.

[24] L Biferale, Guido Boffetta, A Celani, BJ Devenish, A Lanotte, and F Toschi. Multiparticle dispersion in fully developed turbulence. *Physics of Fluids*, 17(11):111701, 2005.

[25] JF Hackl, Pui-Kuen Yeung, and BL Sawford. Multi-particle and tetrad statistics in numerical simulations of turbulent relative dispersion. *Physics of Fluids*, 23(6):065103, 2011.

[26] Enrico Pitton, Cristian Marchioli, Valentina Lavezzo, Alfredo Soldati, and Federico Toschi. Anisotropy in pair dispersion of inertial particles in turbulent channel flow. *Physics of Fluids*, 24(7):073305, 2012.

[27] Juan Ignacio Polanco, Ivana Vinkovic, Nickolas Stelzenmuller, Nicolas Mordant, and Mickaël Bourgoin. Relative dispersion of particle pairs in turbulent channel flow. *International Journal of Heat and Fluid Flow*, 71:231–245, 2018.